THE JOURNAL OF PHYSICAL CHEMISTRY LETTERS
A JOURNAL OF THE AMERICAN CHEMICAL SOCIETY

pubs.acs.org/JPCL

Letter

Resolving Resonant Electronic States in Chiral Metal Complexes by Raman Optical Activity Spectroscopy

Tao Wu,* Josef Kapitán,* and Petr Bouř*

Cite This: *J. Phys. Chem. Lett.* 2022, 13, 3873−3877

Read Online

ACCESS | Metrics & More | Article Recommendations | Supporting Information

ABSTRACT: Chiral metal complexes exhibit rich photophysical properties and are important for applications ranging from biosensing to photocatalysis. We present a combined experimental and computational approach leading to information about energies and transition moments of excited electronic states, documented on two chiral metal complexes. The experimental protocol for measurement of the resonance Raman optical activity comprises multiple techniques, i.e., absorption, circular dichroism, and polarized and differential Raman scattering. An accurate formula for subtraction of the interfering circular dichroism/polarized Raman scattering effect is given. An analysis of the spectra based on density functional theory calculations unveils the geometric and electronic structures of the molecules. Such insight into molecular electronic states of chromophores may be useful for understanding and tuning photochemical properties of metal-containing complexes, biomolecules, and supramolecules.

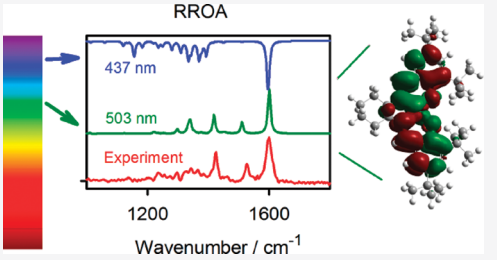

Knowledge of the dynamics and structure of photochemically active excited states in a metal complex is important for tuning their molecular properties in photochemical applications.[1,2] Resonance Raman scattering not only probes the ground-state structure but also reflects the excited-state structure. Dependence of the intensities upon the excitation wavelength provides us with information about state energies, transition dipoles, and molecular potential energy surfaces. The "resonance" when the energy of the photon is close to a difference of molecular electronic levels can be conveniently used, for example, in conformational studies of peptides, where smaller sample amounts are needed than in conventional spectroscopies.[3] The resonance may have even a bigger potential for explorations of molecular vibrational Raman optical activity (ROA).[4] A typical realm of ROA studies consists of biologically relevant systems, such as saccharides, proteins, nucleic acids, but also whole viruses.[5,6]

The resonance not only increases the differential ROA and total Raman signals but also their ratio. The ratio is usually referred to as the (normalized) circular intensity difference, CID = $(I_R - I_L)/(I_R + I_L)$,[7] where I_R and I_L are detected intensities of the right and left circularly polarized light and the sample is irradiated by unpolarized light. In resonance, the vibrational transitions borrow the larger chirality of the electronic transitions, and CID (typically $\sim 10^{-4}$) increases about 10 times.[4,8,9]

First resonance ROA (RROA) spectra were reported in the 1990s.[10] As time went by, RROA found a range of applications, including gases,[11,12] complexes,[13] nanotubes,[14] vitamins,[15] aggregated dyes,[16] and proteins.[17−19] Until recently, however, some samples never provided RROA because the spectra were masked by another phenomenon, a combination of electronic circular dichroism and circularly polarized Raman scattering.[20−22] The observed $I_R - I_L$ imbalance originates in circular dichroism, with different absorption of left and right circularly polarized light, and is particularly strong for metal complexes.[21,2324] This imbalance is further changed during Raman scattering; we therefore refer to the whole phenomenon as ECD-Raman.[9] The recorded $I_R - I_L$ signal is thus a mixture of "true" RROA and ECD-Raman.

Only the latest works proved that the ECD-Raman contribution can be predicted and controlled.[20] In the present study, we use an improved ECD-Raman formula and correct the Raman and ROA intensities for autoabsorption (cf. Supporting Information), so that accurate RROA spectra can be obtained. Quantum chemical simulations then reveal unique information about the geometry, electronic excited states, and local molecular moieties.

The two investigated molecules comprise a cobalt catalyst (BuCo) and a newly synthesized tetracopper complex (cubane; Figure 1). The first molecule belongs to a family of similar compounds widely used in asymmetric catalysis and also studied in connection with molecular chirality.[20,24] Its relatively small molecular size facilitates the theoretical analysis. The second molecule was made from a poly-β-diketone ligand[25] and serves

Received: March 4, 2022
Accepted: April 21, 2022
Published: April 25, 2022

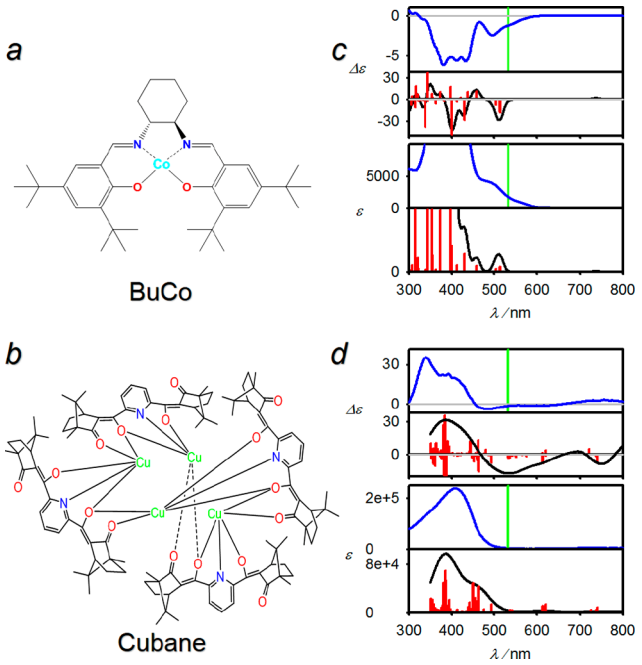

Figure 1. Two model complexes and their electronic spectra. (a and b) (*R*,*R*)-(−)-*N*,*N*′-Bis(3,5-di-*tert*-butylsalicylidene)-1,2-cyclohexanediaminocobalt(II) (*R*-BuCo) and the tetrametallic copper-(II) complex [*R*-cubane, on the basis of *R*-(+)-camphor]. (c and d) Corresponding absorption (ε) and ECD ($\Delta\varepsilon$) spectra of the experiment (blue) and DFT computations (black). The position of the 532 nm laser excitation is indicated by the green line, and individual computed transitions are marked by the red lines.

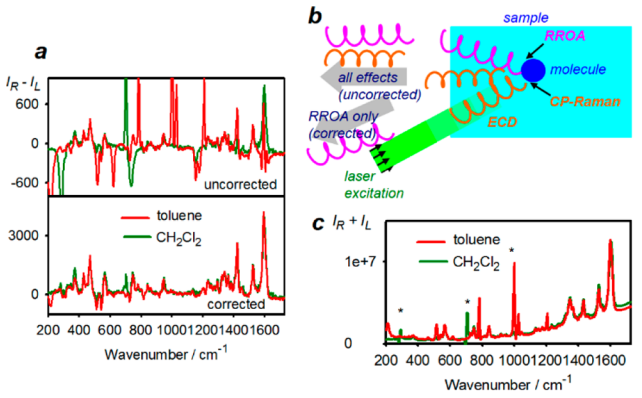

Figure 2. Extraction of the molecular RROA signal. (a) *R*-BuCo ROA spectra measured in the two solvents, before and after the ECD-Raman subtraction. (b) Three main chirality events in the sample: (1) originally unpolarized light passing through the sample is circularly polarized as a result of electronic circular dichroism; (2) circular polarization is changed during Raman scattering ("CP-Raman"); and (3) finally, RROA of chiral molecules contributes to the total $I_R - I_L$ circular polarization difference. (c) *R*-BuCo Raman spectra. Asterisks (∗) indicate incomplete subtraction of solvent Raman bands.

as an example of more complicated systems, i.e., metallo-supramolecular framework.[13,26]

Both complexes are paramagnetic, with multiplicities M(BuCo) = 2 and M(cubane) = 5. Even at low concentrations, their solutions are dark, and at 532 nm, they exhibit a relatively strong ECD signal (Figure 1, right). This is, in general, a good condition for resonance RROA.[9,27] The calculated spectra agree reasonably well with the experimental spectra, within errors usual for the time-dependent density functional theory (TDDFT).[28] The error and low spectral resolution, however, prohibit determination of which electronic state(s) are responsible for the resonance effect solely from the theory.

The process of obtaining the RROA differential signal is relatively complicated and is indicated for BuCo in panels a and b of Figure 2. Raw ROA spectra or more precisely measured $I_R - I_L$ differences are quite different for toluene and dichloromethane as a solvent. The solvent Raman scattering combines with ECD of the solute, producing "false" signals also in place of solvent Raman bands.[20−22,24] With our procedure, we could nevertheless subtract this ECD-Raman part and, thus, arrive at a pure RROA signal.

The derivation is given in detail in the Supporting Information. Briefly, to obtain RROA spectra, we also measured absorption and ECD to obtain natural molar extinction coefficients at the incident (e, Δe) and scattered (e', $\Delta e'$) wavelengths. The laser was focused in the sample close to the front cell window to minimize the ECD-active only path length ($L' \sim 0$; cf. Supporting Information). Then, the ECD-Raman intensity was calculated as

$$I_{\mathrm{dif}}^{\mathrm{u}} = \frac{1 - [1 + (e + e')CL]e^{-(e+e')CL}}{2(e + e')(1 - e^{-(e+e')CL})}(I_{\mathrm{dif}}^{R}\Delta e + I_{\mathrm{sum}}^{R}\Delta e') \quad (1)$$

where C is the molar complex concentration, L is the Raman-active path length, and I_{sum}^{R} and I_{dif}^{R} are total and differential Raman intensities obtained with right circularly polarized excitation light. The subtraction of ECD-Raman to obtain RROA based on eq 1 works for a wide range of absorptions and relative ECD-Raman/RROA signal ratios, as also qualitatively investigated before.[22] In the derivation, we only assumed that ECD is much weaker than absorption, which is always true for molecules.

Corresponding Raman spectra (Figure 2c) exhibit a broad background at higher frequencies, coming from a fluorescence band centered around 3500 cm^{-1}. The RROA/Raman normalized CID ratio for the strongest C=C stretching 1600 cm^{-1} band is 4.8×10^{-4}, which is not extreme but slightly above the strongest non-resonance ROA signals produced by rigid organic molecules, such as camphor or α-pinene.[4]

At the higher frequency part, the RROA spectrum (lower part of Figure 2a) approximately obeys the single electronic state theory,[27] which says that CID should be equal to $-g/2$, where g is Kuhn's dissymmetry factor, i.e., ratio of ECD and absorption intensities of the one resonant electronic transition. Indeed, in our case, $-g/2 = 4.1 \times 10^{-4}$ at 532 nm. At lower wavenumbers, negative bands appear as well (e.g., Co−N and Co−O stretching containing modes at 513 and 544 cm^{-1}; see also Table S2 of the Supporting Information). This indicates the involvement of more than one electronic transition in RROA.

Although the TDDFT calculations reproduced the main experimental features in Figure 1, their accuracy is not sufficient to point out the actual resonating state(s). This can be done more precisely on the basis of the RROA spectra. The Raman and ROA spectra calculated in the pre-resonance approximation by the Gaussian software[29] already very much depend upon the color of the excitation light (Figure 3a). Many kinds of intensity patterns are produced, depending upon which part of the molecule is excited, and the intensity magnitudes vary by several orders, depending upon how close the light frequency is to the

https://doi.org/10.1021/acs.jpclett.2c00653
J. Phys. Chem. Lett. 2022, 13, 3873−3877

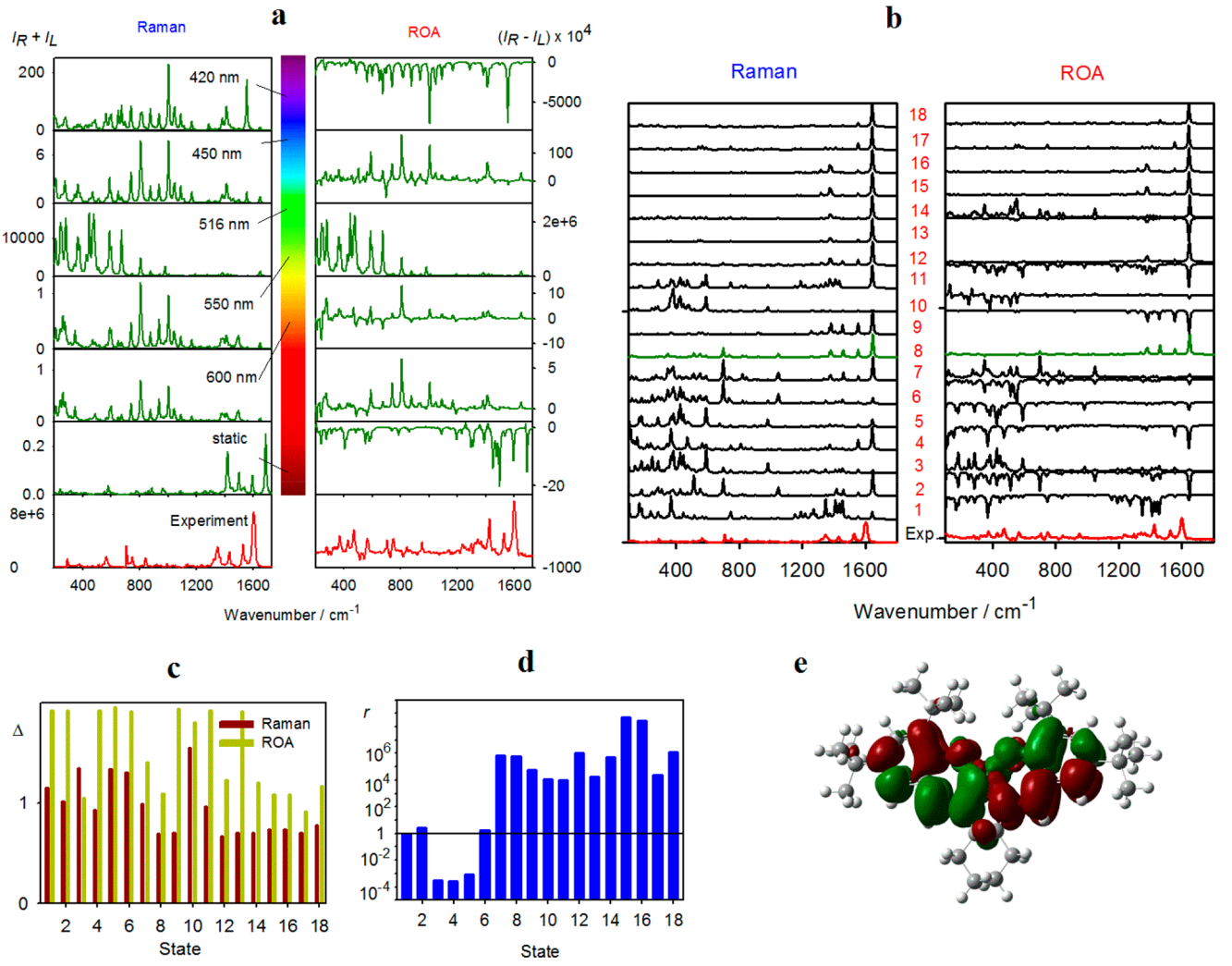

Figure 3. Assignment of the resonating electronic transition in the BuCo complex. (a) Raman and ROA spectra calculated for different excitation wavelengths do not provide much specific information. (b) This was obtained from spectral contributions from individual transitions (red numbers), for the 532 nm excitation, normalized to the biggest band, with calculated wavenumbers scaled by 0.977, and the experiment for CH_2Cl_2 solution. (c) Integral spectra errors ($\Delta \int |S_{exp} - S_{cal}| d\nu / \int |S_{cal}| d\nu$, for spectra normalized to unit area) and (d) relative Raman intensities (r) for different states. (e) Transition charge density for the electronic transition number 8, most likely dominating the RROA effect.

electronic frequency. However, none of them fully reproduces the experiment. The plain pre-resonance TDDFT method does not seem to be able to provide realistic simulated spectra because of the approximations involved. For example, the static limit (light wavelength goes to infinity) provides one sign ROA, as in the experiment, but the sign is opposite.

More detailed and realistic insight is obtained when we simulate contributions of the electronic transitions to Raman and ROA spectra individually. The normalized spectral intensities stemming from the first 18 transitions to the lowest energy electronic states are compared to the experimental spectra in Figure 3b. Only transition 8 provides a realistic pattern, for both Raman and ROA. The agreement can be quantified if we calculate the integral spectral error between the normalized shapes (Figure 3c). In the vicinity of the 532 nm excitation, this transition provides the smallest error. When the resonating states are assigned, one must take into account not only spectral shapes (Figure 3b) but also the enhancement (absolute strength) of the signal (Figure 3d). For example, spectral intensity coming from states 1−6 is by several orders smaller than that from the others. In this respect, the assignment of state 8 to the resonance is consistent, because it provides a very strong signal. States 15 and 16 give even stronger enhancements but are also much further from the excitation frequency. They may contribute to the measured signal, but currently, the extent of this contribution cannot be estimated precisely. All of these transitions (8, 12, 15, and 16) comprise a charge transfer across the aromatic system of the ligands through the cobalt d-electron system. This can be seen in Figure 3e where the transition electron density for state 8 is plotted. This localization of the electronic transitions also explains the relatively selective enhancement of the C═C aromatic bond stretching bands at 1603 cm^{-1}.

The metallo-supramolecule (CCDC database registered number 2043703 for *R*-cubane) behaves similarly to BuCo; i.e., RROA is masked by the ECD-Raman effect, and true RROA must be extracted using eq 1. However, the g factor at 532 nm is smaller ($-g/2 = 2.7 \times 10^{-4}$), and the ROA spectrum has many positive and negative bands, with CID $\sim 1 \times 10^{-4}$. Only for the strongest signal at 1556 cm^{-1}, CID is somewhat higher, $\sim 3.8 \times 10^{-4}$. The weakness and bisignate character suggest that the effect of resonance is more complex for the copper compound.

https://doi.org/10.1021/acs.jpclett.2c00653
J. Phys. Chem. Lett. 2022, 13, 3873−3877

Indeed, the spectra calculated at the 532 nm pre-resonance conditions using molecular fragments already reasonably well reproduced the experiment (Figure 4a). The C═O stretching

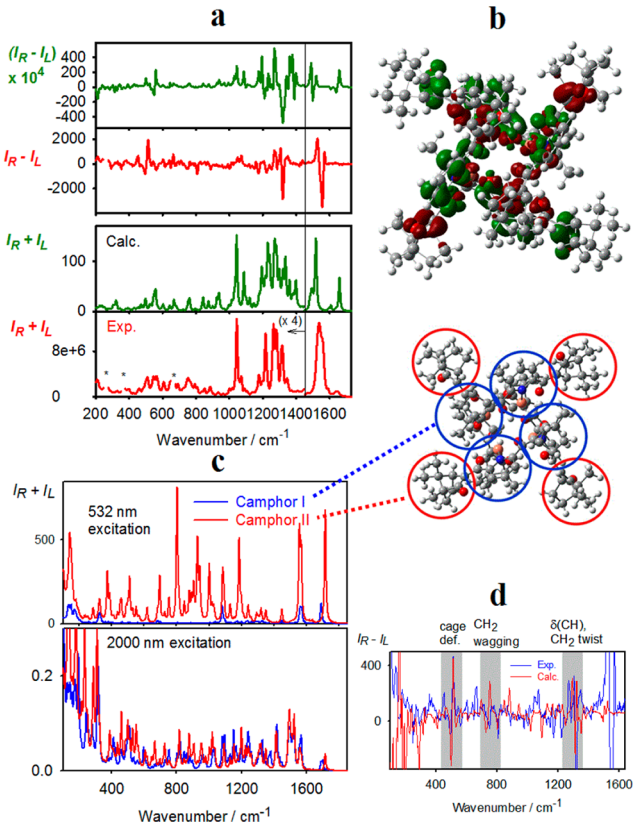

Figure 4. Raman and RROA of *R*-cubane. (a) Calculated (B3LYP/6-311++G**/CCT/PCM) and experimental spectra. For better visibility, calculated intensities below 1450 cm^{-1} were multiplied by 4. (b) Transition charge density of electronic transition number 46, identified as the dominant transition for the resonance Raman/RROA effect. (c) Raman intensities coming from camphor atoms, generated separately for the two camphor residue kinds indicated, at 532 and 2000 nm excitations. (d) Calculated RROA with the camphor atoms only and the experiment.

signal (>1590 cm^{-1}; cf. Supporting Information for the mode assignment) is calculated stronger than observed. The RROA spectrum is dominated by a W-shape pattern around 1535 cm^{-1} of predominantly C═C stretching in the ketone part of the molecule, which is reproduced by the calculation. Within 1100−1450 cm^{-1}, there are about 190 fundamental vibrational transitions, mostly assigned to CH bending but also to C−C stretching and other deformations. The pyridine breathing mode (1044 cm^{-1}) gives a relatively strong Raman intensity; RROA in this region is relatively weak and predominantly positive. The last lowest frequency RROA feature, a W shape within 400−520 cm^{-1}, belongs to delocalized vibrations spanning the whole molecule, and the computation reproduces it quite well.

For cubane, more electronic transitions occur in the vicinity of the 532 nm excitation line. For example, within 490−550 nm, the calculations suggest 3 transitions for BuCo but 13 for cubane. The analysis of the contributions of individual excited electronic states to Raman and ROA spectra suggests that state number 46 (transition wavelength calculated at 464 nm) is the best candidate for the dominant contributor to Raman/RROA intensities, giving a Raman shape close to the experiment. Its RROA is also negative, as observed, and the overall enhancement is extremely high. Its transition charge density is visualized in Figure 4b. In the transition, all four ligands with all of the double-bond electronic systems and copper d electrons participate, which presumably makes its contribution to the Raman signal so strong.

A very interesting and potentially useful feature of resonance Raman and ROA spectroscopy is documented in Figure 4c. Here, we generate Raman intensities coming from the two types of the camphor residues: camphors attached through the carbonyl group to a copper atom (I) and the other type (II). At the 2000 nm excitation (non-resonance case), the two camphor residue types contribute about equally, which corresponds to their similar chemical and optical nature. At the 532 nm excitation, however, type II carbonyl groups are heavily involved in the resonance (cf. also the transition charge density; Figure 4b), and their signal dominates the spectrum. The carbonyl group in type I bonded to copper apparently loses the ability of the π electrons to participate at the electronic transitions with energies close to the laser excitation. In comparison to the main Raman and RROA bands at ~1556 cm^{-1}, the camphor moieties do not contribute to the RROA spectra so much; however, they can be identified in the experimental spectrum, and the simulated shape agrees well with the observation (Figure 4d).

The RROA spectra of the metal complexes thus seem to be capable of distinguishing states close in energy, which could not be resolved by other means. The electronic spectra provided limited resolution only, and the errors of computed electronic transition energies and pre-resonance spectral intensities were too large. We show that delocalized electronic states, spread over all of the ligands and with a significant participation of metal d electrons, are the most important for the resonance intensities. Theoretical analysis revealed an interesting possibility to "light" a particular molecular moiety, in this case, different camphor residues, by the laser excitation frequency. The probing of electronic excited states may be used in molecular studies concerning bioinorganic and metallo-supramolecular chemistry, asymmetric catalysis, or photochemically active materials.

■ ASSOCIATED CONTENT

Supporting Information

The Supporting Information is available free of charge at https://pubs.acs.org/doi/10.1021/acs.jpclett.2c00653.

Details of the measurements and calculations, RROA theory, ECD-Raman spectra extraction, and synthesis and structure characterization of the cubane complex (PDF)

Transparent Peer Review report available (PDF)

■ AUTHOR INFORMATION

Corresponding Authors

Tao Wu − *Institute of Organic Chemistry and Biochemistry, Academy of Sciences, 16610 Prague, Czech Republic;* orcid.org/0000-0002-0244-3046; Email: wu@uochb.cas.cz

Josef Kapitán − *Department of Optics, Palacký University Olomouc, 77146 Olomouc, Czech Republic;* orcid.org/0000-0002-1916-9186; Email: kapitan@optics.upol.cz

Petr Bouř − *Institute of Organic Chemistry and Biochemistry, Academy of Sciences, 16610 Prague, Czech Republic;* orcid.org/0000-0001-8469-1686; Email: bour@uochb.cas.cz

https://doi.org/10.1021/acs.jpclett.2c00653
J. Phys. Chem. Lett. 2022, 13, 3873−3877

Complete contact information is available at:
https://pubs.acs.org/10.1021/acs.jpclett.2c00653

Funding

This work was funded by the Grant Agency (22-04669S) and the Ministry of Education (CZ.02.1.01/0.0/0.0/16_019/0000729) of the Czech Republic.

Notes

The authors declare no competing financial interest.

■ ACKNOWLEDGMENTS

The authors thank David Kopečný, Palacký University Olomouc, for the help with ECD spectra measurement.

■ REFERENCES

(1) Zedler, L.; Mengele, A. K.; Ziems, K. M.; Zhang, Y.; Wächtler, M.; Gräfe, S.; Pascher, T.; Rau, S.; Kupfer, S.; Dietzek, B. Unraveling the Light-Activated Reaction Mechanism in a Catalytically Competent Key Intermediate of a Multifunctional Molecular Catalyst for artificial Photosynthesis. *Angew. Chem., Int. Ed.* **2019**, *58*, 13140−13148.

(2) Sutton, J. J.; Preston, D.; Traber, P.; Steinmetzer, J.; Wu, X.; Kayal, S.; Sun, X. Z.; Crowley, J. D.; George, M. W.; Kupfer, S.; Gordon, K. C. Excited-State Switching in Rhenium(I) Bipyridyl Complexes with Donor−Donor and Donor−Acceptor Substituents. *J. Am. Chem. Soc.* **2021**, *143*, 9082−9093.

(3) Asher, S. A.; Ianoul, A.; Mix, G.; Boyden, M. N.; Karnoup, A.; Diem, M.; Schweitzer-Stenner, R. Dihedral psi angle dependence of the amide III vibration: A uniquely sensitive UV resonance Raman secondary structural probe. *J. Am. Chem. Soc.* **2001**, *123*, 11775−11781.

(4) Nafie, L. A. *Vibrational Optical Activity: Principles and Applications*; Wiley: Chichester, U.K., 2011; DOI: 10.1002/9781119976516.

(5) Barron, L. D.; Blanch, E. W.; McColl, I. H.; Syme, C. D.; Hecht, L.; Nielsen, K. Structure and behaviour of proteins, nucleic acids and viruses from vibrational Raman optical activity. *J. Spectrosc.* **2003**, *17*, 101−126.

(6) Krupová, M.; Kessler, J.; Bouř, P. Recent Trends in Chiroptical Spectroscopy: Theory and Applications of Vibrational Circular Dichroism and Raman Optical Activity. *ChemPlusChem* **2020**, *85*, 561−575.

(7) Barron, L. D. *Molecular Light Scattering and Optical Activity*, 2nd ed.; Cambridge University Press: Cambridge, U.K., 2004; DOI: 10.1017/CBO9780511535468.

(8) Dudek, M.; Zajac, G.; Kaczor, A.; Baranska, M. Aggregation-Induced Resonance Raman Optical Activity (AIRROA) and Time-Dependent Helicity Switching of Astaxanthin Supramolecular Assemblies. *J. Phys. Chem. B* **2016**, *120*, 7807−7814.

(9) Zając, G.; Bouř, P. Measurement and Theory of Resonance Raman Optical Activity for Gases, Liquids, and Aggregates. What It Tells about Molecules. *J. Phys. Chem. B* **2022**, *126*, 355−367.

(10) Vargek, M.; Freedman, T. B.; Lee, E.; Nafie, L. A. Experimental observation of resonance Raman optical activity. *Chem. Phys. Lett.* **1998**, *287*, 359−364.

(11) Šebestík, J.; Kapitán, J.; Pačes, O.; Bouř, P. Diamagnetic Raman Optical Activity of Chlorine, Bromine, and Iodine Gases. *Angew. Chem., Int. Ed.* **2016**, *55*, 3504−3508.

(12) Šebestík, J.; Bouř, P. Observation of Paramagnetic Raman Optical Activity of Nitrogen Dioxide. *Angew. Chem., Int. Ed.* **2014**, *53*, 9236−9239.

(13) Merten, C.; Li, H.; Nafie, L. A. Simultaneous Resonance Raman Optical Activity Involving Two Electronic States. *J. Phys. Chem. A* **2012**, *116*, 7329−7336.

(14) Magg, M.; Kadria-Vili, Y.; Oulevey, P.; Weisman, R. B.; Bürgi, T. Resonance Raman Optical Activity Spectra of Single-Walled Carbon Nanotube Enantiomers. *J. Phys. Chem. Lett.* **2016**, *7*, 221−225.

(15) Machalska, E.; Zajac, G.; Gruca, A.; Zobi, F.; Baranska, M.; Kaczor, A. Resonance Raman Optical Activity Shows Unusual Structural Sensitivity for Systems in Resonance with Multiple Excited States: Vitamin B12 Case. *J. Phys. Chem. Lett.* **2020**, *11*, 5037−5043.

(16) Zajac, G.; Kaczor, A.; Pallares Zazo, A.; Mlynarski, J.; Dudek, M.; Baranska, M. Aggregation-Induced Resonance Raman Optical Activity (AIRROA): A New Mechanism for Chirality Enhancement. *J. Phys. Chem. B* **2016**, *120*, 4028−4033.

(17) Fujisawa, T.; Leverenz, R. L.; Nagamine, M.; Kerfeld, C. A.; Unno, M. Raman Optical Activity Reveals Carotenoid Photoactivation Events in the Orange Carotenoid Protein in Solution. *J. Am. Chem. Soc.* **2017**, *139*, 10456−10460.

(18) Sgammato, R.; Herrebout, W.; Johannessen, C. Resonance Raman optical activity of the imidazole−Myoglobin complex: Titrating enhancement. *J. Raman Spectrosc.* **2019**, *50*, 1905−1913.

(19) Bogaerts, J.; Johannessen, C. On/off resonance Raman optical activity of human serum transferrin. *J. Raman Spectrosc.* **2019**, *50*, 641−646.

(20) Wu, T.; Li, G.; Kapitán, J.; Kessler, J.; Xu, Y.; Bouř, P. Two Spectroscopies in One: Interference of Circular Dichroism and Raman Optical Activity. *Angew. Chem. Int. Ed.* **2020**, *59*, 21895−21898.

(21) Li, G.; Alshalalfeh, M.; Yang, W.; Cheeseman, J. R.; Bouř, P.; Xu, Y. Can One Measure Resonance Raman Optical Activity? *Angew. Chem. Int. Ed.* **2021**, *60*, 22004−22009.

(22) Machalska, E.; Zajac, G.; Wierzba, A. J.; Kapitán, J.; Andruniów, T.; Spiegel, M.; Gryko, D.; Bouř, P.; Baranska, M. Recognition of the True and False Resonance Raman Optical Activity. *Angew. Chem. Int. Ed.* **2021**, *60*, 21205−21210.

(23) Tomeček, J.; Bouř, P. Density Functional Computations of Vibrational Circular Dichroism Spectra beyond the Born−Oppenheimer Approximation. *J. Chem. Theory Comput.* **2020**, *16*, 2627−2634.

(24) Li, G.; Kessler, J.; Cheramy, J.; Wu, T.; Poopari, M. R.; Bouř, P.; Xu, Y. Transfer and Amplification of Chirality within the 'Ring of Fire' Observed in Resonance Raman Optical Activity Experiments. *Angew. Chem. Int. Ed.* **2019**, *58*, 16495−16498.

(25) Wu, T.; You, X. Exciton Coupling Analysis and Enolization Monitoring by Vibrational Circular Dichroism Spectra of Camphor Diketones. *J. Phys. Chem. A* **2012**, *116*, 8959−8964.

(26) Clegg, J. K.; Li, F.; Lindoy, L. F. Oligo-β-diketones as versatile ligands for use in metallo-supramolecular chemistry: Recent progress and perspectives. *Coord. Chem. Rev.* **2022**, *455*, 214355.

(27) Nafie, L. A. Theory of resonance Raman optical activity: The single electronic state limit. *Chem. Phys.* **1996**, *205*, 309−322.

(28) Furche, F.; Ahlrichs, R. Adiabatic time-dependent density functional methods for excited state properties. *J. Chem. Phys.* **2002**, *117*, 7433−7447.

(29) Frisch, M. J.; Trucks, G. W.; Schlegel, H. B.; Scuseria, G. E.; Robb, M. A.; Cheeseman, J. R.; Scalmani, G.; Barone, V.; Petersson, G. A.; Nakatsuji, H.; Li, X.; Caricato, M.; Marenich, A. V.; Bloino, J.; Janesko, B. G.; Gomperts, R.; Mennucci, B.; Hratchian, H. P.; Ortiz, J. V.; Izmaylov, A. F.; Sonnenberg, J. L.; Williams-Young, D.; Ding, F.; Lipparini, F.; Egidi, F.; Goings, J.; Peng, B.; Petrone, A.; Henderson, T.; Ranasinghe, D.; Zakrzewski, V. G.; Gao, J.; Rega, N.; Zheng, G.; Liang, W.; Hada, M.; Ehara, M.; Toyota, K.; Fukuda, R.; Hasegawa, J.; Ishida, M.; Nakajima, T.; Honda, Y.; Kitao, O.; Nakai, H.; Vreven, T.; Throssell, K.; Montgomery, J. A., Jr.; Peralta, J. E.; Ogliaro, F.; Bearpark, M. J.; Heyd, J. J.; Brothers, E. N.; Kudin, K. N.; Staroverov, V. N.; Keith, T. A.; Kobayashi, R.; Normand, J.; Raghavachari, K.; Rendell, A. P.; Burant, J. C.; Iyengar, S. S.; Tomasi, J.; Cossi, M.; Millam, J. M.; Klene, M.; Adamo, C.; Cammi, R.; Ochterski, J. W.; Martin, R. L.; Morokuma, K.; Farkas, O.; Foresman, J. B.; Fox, D. J. *Gaussian 16, Revision A.03*; Gaussian, Inc.: Wallingford, CT, 2016.